LARGE EDDY SIMULATIONS FOR DISPERSED BUBBLY FLOWS

T. Ma, T. Ziegenhein, D. Lucas, E. Krepper

Helmholtz-Zentrum Dresden-Rossendorf
Institute of Fluid Dynamics, 01314 Dresden, Germany

J. Fröhlich

Technische Universität Dresden
Institut für Strömungsmechanik, 01062 Dresden, Germany

tian.ma@hzdr.de

ABSTRACT

In this paper we present detailed Euler-Euler Large Eddy Simulations (LES) of dispersed bubbly flow in a rectangular bubble column. The motivation of this study is to investigate potential of this approach for the prediction of bubbly flows, in terms of mean quantities. The set of physical models describing the momentum exchange between the phases was chosen according to previous experiences of the authors. Experimental data, Euler-Lagrange LES and unsteady Euler-Euler Reynolds-Averaged Navier-Stokes model are used for comparison. It was found that the presented modelling combination provides good agreement with experimental data for the mean flow and liquid velocity fluctuations. The energy spectrum made from the resolved velocity from Euler-Euler LES is presented and discussed.

1. INTRODUCTION

Many flow regimes in nuclear engineering and chemical engineering are gas-liquid flows with a continuous liquid phase and a dispersed gaseous phase. Computational Fluid Dynamics (CFD) simulations become more and more important for the design of the related processes, for process optimization as well as for safety considerations. Because of the large scales that need to be considered for such purposes, the two-fluid or multi-fluid approach is often the most suitable framework. During the last years, clear progress was achieved for modelling dispersed flows such as bubbly flows. At Helmholtz-Zentrum Dresden-Rossendorf, in cooperation with ANSYS, the inhomogeneous Multiple Size Group (iMUSIG) model was developed (Krepper et al. 2008). It is based on bubble size classes for the mass balance as well as for the momentum balance. This model has been currently extended by adding a continuous gas phase for a generalized two-phase flow (GENTOP) (Hänsch et al. 2012). The aim of the GENTOP concept is to treat both unresolved and resolved multiphase structures. This study concentrates in the turbulence modelling in the unresolved structures.

Turbulence in the liquid phase is an important issue in bubbly flows as it has a strong influence on the local distribution of the dispersed phase. Compared to the liquid phase the influence of the turbulence in the gas phase is generally negligible because of the low density of the gas and the small dimensions of bubbles.

A bubble column provides a good experimental system for the study of turbulent phenomena in bubbly flows. In bubble columns a wide range of length and time scales exists on which turbulent mixing takes place. The largest turbulence scales are comparable in size to the characteristic length of the mean flow and depend on reactor geometry and boundary conditions. The smaller scales depend on the bubble dynamics and hence are proportional to the bubble diameter. In bubbly flows, the small scales are responsible for the dissipation of the turbulent kinetic energy as in single-phase flow, but the bubbles can also generate back-scatter, i.e. energy transfer from smaller to larger scales (Dhotre et al. 2013). The combination of both effects can yield an overall enhancement or attenuation of the turbulence intensity.

In the present paper the effect of turbulence modelling is investigated. In the CFD simulations of bubble columns, Reynolds-Averaged Navier-Stokes (RANS) models are used for modelling turbulence in the traditional way, using isotropic closures without resolution of turbulent scales. Large Eddy Simulation (LES) offers the possibility to resolve the large-scale anisotropic turbulent motion and to model the small scales with a Subgrid-Scale (SGS) model. The Euler-Euler LES (Eu-Eu-LES) of the bubbly flow is performed in this work. In particularly, the SGS turbulent kinetic energy in LES will be estimated for zero-equation SGS models to improve the prediction.

2. EXPERIMENTAL DATA

The simulations are carried out for a rectangular water/air bubble column at ambient pressure and are compared with the experimental data for two different gas superficial velocities at the inlet (Akbar et al. 2012). A schematic sketch of the experimental setup is shown in Figure 1. Its width, depth and height are 240, 72 and 800 mm, respectively and the water level is 700 mm. A distributor plate containing 35 evenly spaced needles with an inner diameter of 0.51mm was at the bottom of the column. Measurements were performed for two superficial velocities 3 mm/s (Case 1) and 13 mm/s (Case 2) and took place 500 mm above distributor plate (z = 500 mm) in the centre plane (y = 36mm). More details are provided in the cited reference.

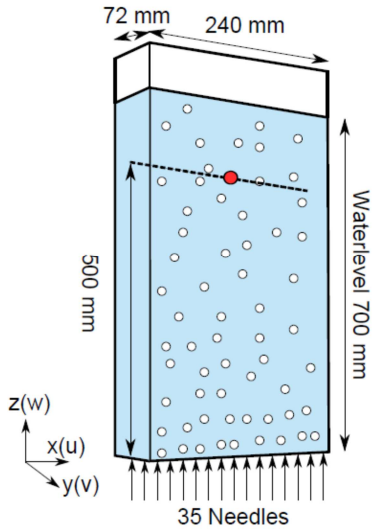

Fig. 1 Schematic representation of the experiment of Akbar et al. (2012)
The broken line in the figure shows the measurement position. The marker on that line is the measurement point for the results presented in Figure 9 and 10.

3. PHYSICAL MODELING

3.1 Euler-Euler Approach

In this work the Euler-Euler two-fluid model is used. The conservation equations have been discussed at length in a number of books, such as Ishii & Hibiki (2011), and a broad consensus has been reached. Governing equations using this approach are the continuity and momentum equations, without mass transfer and sources between the phases.

$$\frac{\partial}{\partial t}(r_\alpha \rho_\alpha) + \nabla \cdot (r_\alpha \rho_\alpha \overline{\boldsymbol{u}}_\alpha) = 0 \tag{1}$$

$$\frac{\partial (r_\alpha \rho_\alpha \overline{\boldsymbol{u}}_{\boldsymbol{\alpha}})}{\partial t} + \nabla \cdot (r_\alpha \rho_\alpha \overline{\boldsymbol{u}}_{\boldsymbol{\alpha}} \overline{\boldsymbol{u}}_{\boldsymbol{\alpha}}) = -\nabla (r_\alpha \mu_\alpha \overline{\boldsymbol{S}}_{\boldsymbol{\alpha}}) - r_\alpha \nabla p + r_\alpha \rho_\alpha \boldsymbol{g} + \boldsymbol{M}_{\boldsymbol{\alpha}} - \nabla (r_\alpha \boldsymbol{\tau}_{\boldsymbol{\alpha}}) \tag{2}$$

Here, the lower index α denotes the different phases, which r, ρ, μ and $\overline{\boldsymbol{u}}$ are the volume fraction, density, molecular viscosity and resolved velocity of phase α, respectively, and $\overline{\boldsymbol{S}}$ is the strain rate tensor. The vector $\boldsymbol{M}$ represents the sum of all interfacial forces acting between the phases resulting

from physical effects like drag force, lift force, wall lubrication and turbulent dispersion force. The SGS stress $\boldsymbol{\tau}$, and all interfacial forces have to be modelled, which is discussed below.
(1) and (2) are usually derived by ensemble averaging. However, the same form of the equations is obtained if one performs filtering (volume averaging) of the governing equations (Niceno et al. 2008). This is of practical importance for LES, because it means that the same numerical tools developed for ensemble averaged Euler-Euler equations, can be used for LES.

3.2 Turbulence

3.2.1 Two-phase turbulence

In this study, turbulence is treated differently for the different phases. Because of the low density of the gas, the turbulence in dispersed gas phase is of little relevance and is modelled with a simple zero equation model only. It was found that this model has nearly no influence on the result. For the continuous, liquid phase, LES was used.

3.2.2 LES for continuous liquid phase

Velocities in (1) and (2), $\overline{\boldsymbol{u}}_{\boldsymbol{\alpha}}$, represent the resolved velocity. The corresponding unresolved components are:

$$\boldsymbol{u}'_{\boldsymbol{\alpha}} = \boldsymbol{u}_{\boldsymbol{\alpha}} - \overline{\boldsymbol{u}}_{\boldsymbol{\alpha}} , \tag{3}$$

in which $\boldsymbol{u}_{\boldsymbol{\alpha}}$ is the true velocity of phase α. The SGS stress tensor $\tau_{ij} = \overline{u_i u_j} - \bar{u}_i \bar{u}_j$, is modelled by the Smagorinsky model (Smagorinsky et al. 1963):

$$\tau_{ij}^a = \tau_{ij} - \frac{1}{3}\tau_{kk}\delta_{ij} = -2\nu_{sgs}\bar{S}_{ij} \text{ with } \nu_{sgs} = (C_s\Delta)^2|\bar{S}|, \tag{4}$$

with τ_{ij}^a being the anisotropic (traceless) part of the SGS stress tensor τ_{ij}, and δ_{ij} the Kronecker delta. The SGS viscosity, ν_{sgs}, is a function of the magnitude of the strain rate tensor, $|\bar{S}| = \sqrt{2\bar{S}_{ij}\bar{S}_{ij}}$, and the subgrid length scale is $l = C_s\Delta$. Here, C_s the model constant was chosen to be $C_s = 0.15$, while the filter width Δ was determined by the grid size $\Delta = \sqrt[3]{Vol}$. The trace of the SGS stress tensor τ_{kk} in (4) is added to the filtered pressure $\bar{p}$, resulting in a modified pressure $P = \bar{p} + \frac{\tau_{kk}}{3}$. For wall modelling, the turbulent viscosity close to the walls is damped using the formulation of Shur et al. (2008).

3.2.3 Bubble induced turbulence (BIT)

With the Euler-Euler approach bubbles are not resolved. The resolved part of the velocity field in LES presents only the shear-induced turbulence, which in assumed to be independent of the relative motion of bubbles and liquid. The influence in liquid turbulence caused from the bubbles traveling through the liquid (e.g. bubble wake instability, bubble oscillation) has to be modelled. In two equation RANS models, additional source terms have been developed to describe bubble induced turbulence. The approximation is provided by the assumption that all energy lost by the bubble due to drag is converted to turbulent kinetic energy in the wake of the bubble. Detailed information about the BIT models in RANS can be found in the recent review of Rzehak and Krepper (2013). Such an approach is not suitable for LES with zero equation SGS model, because no transport equation for k is available. Here, we use the common BIT model of Sato et al. (1981). In this model the bubble influence in liquid turbulence is included by an additional extra term to the SGS turbulent viscosity so that:

$$\mu_L^{eff} = \mu_L^{mol} + \mu_L^{sgs} + \mu_L^{bub} \text{ with } \mu_L^{bub} = C_B\rho_L\alpha_G d_B|\boldsymbol{u}_G - \boldsymbol{u}_L| . \tag{5}$$

C_B is here a model constant equal to 0.6, and d_B represents the bubble diameter. In LES, μ_L^{bub} is added directly in the SGS model, without direct contribution in the total turbulent kinetic energy, i.e.

$$\tau_{ij}^a = \left(\tau_{ij} - \frac{1}{3}\tau_{kk}\,\delta_{ij}\right) = -2(\nu_{sgs} + \nu_{BIT})S_{ij}, \tag{6}$$

since τ_{kk} is not computed anyway.

3.3 Interfacial Forces

In the Eulerian two-fluid model the interaction of the bubbles and the liquid phase is modelled through exchange terms between the separate impulse conservation equation of the liquid and the gas phase. They are still subject to discussion in the community and vary between researchers. Table 1 shows a summary of the interfacial transfer models used here. For more details about each model, a complete description of all interfacial transfer is published by Rzehak and Krepper (2013).

Table 1: Interfacial forces models for both cases employed in the present work

Interfacial forces	Drag force	Lift force	Wall force	Turbulent dispersion
Models	Ishii and Zuber (1979)	Tomiyama et al. (2002)	Hosokawa et al. (2002)	None

Turbulent Dispersion Force

The turbulent dispersion force is the result of the turbulent fluctuations of liquid velocity. In URANS simulations, this part should be modelled; because only a very small part of turbulence is calculated. In LES, velocities are decomposed into a resolved part and a SGS part, which means the resolved part of the turbulent dispersion is explicitly calculated. The unresolved part in SGS has little influence on bubble dispersion, if the bubble size is in the scale of the filter size (Niceno et al. 2008).

4. SIMULATION SETUP

4.1 Polydispersity and iMUSIG

The measured bubble size distributions at the inlet and measurement plane are given in Figure 2. As can be seen, the bubble size distribution for the two cases near the sparger and 500 mm above the sparger is almost the same. Therefore, coalescence and break-up will be neglected. For modelling the polydispersity, the inhomogeneous multiple size group (iMUSIG) model as introduced by Krepper et al. (2008) assigns different velocity groups to the bubble classes used in the MUSIG model. Each velocity group has therefore its own velocity field. This is important, to describe effects like the bubble size dependent movement of the gas phase caused by the lift force. In the present case, the bubble classes are chosen in such a way that the bubble size distributions, as shown in Figure 2, are split into two contributions at the diameter where the lift force changes its sign, which is d_B = 5.8 mm. The resulting bubble classes for Case 2 can be found in Table 2. In Case 1 bubbles are treated as monodisperse with d_B = 4.37 mm, because almost all bubbles have a positive lift coefficient, so that there is no need for considering different velocity groups.

Table 2: Bubble classes employed in Case 2

	d_B	α	$Eo_\perp$	C_L
Bubble Class 1	5.3 mm	0.63 %	3	0.288
Bubble Class 2	6.3 mm	0.37 %	7.3	-0.116

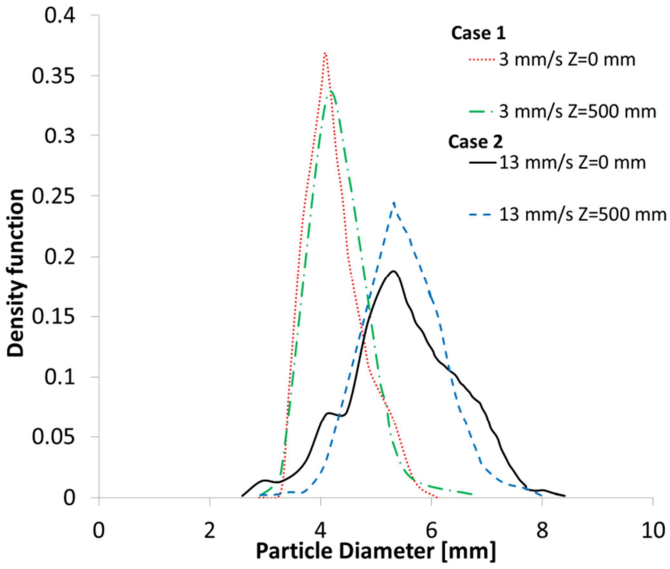

Fig. 2 Measured bubble size distribution at z = 0 and 500 mm (Akbar et al. 2012).

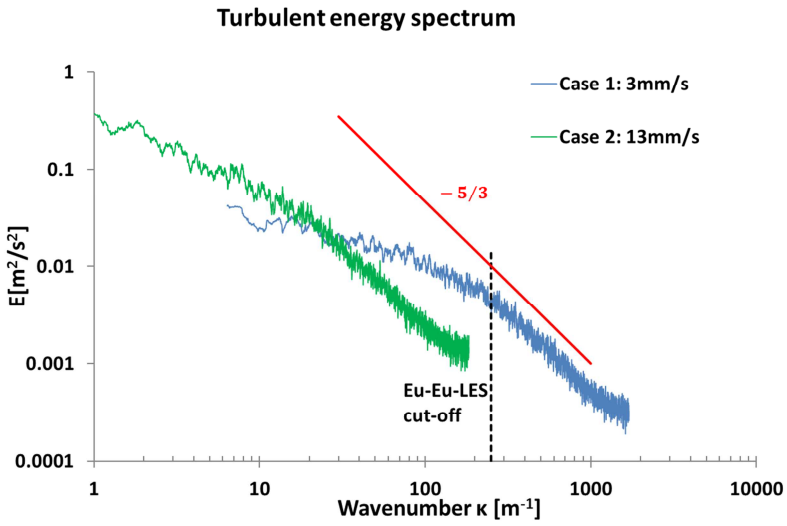

Fig. 3: Turbulent energy spectrum of fluctuating vertical velocity.

4.2 Numerical Conditions

Grid Requirement

The rectangular bubble column was discretized with uniform cubic cells of $\Delta x = \Delta y = \Delta z = 4$ mm, resulting in about 200000 cells, overall. The spatial resolution is in the order of the bubble size ($d^* = \frac{\Delta x}{d_B} \sim 1$). The Euler-Euler method is a volume-averaging approach without using a point-force approximation for the interaction between bubbles and liquid. Hence, there is no strict requirement, like for most of the bubble tracking methods, that the grid size should be at least 50% larger than the (physical) bubble diameter when modelling interfacial forces (Milelli et al. 2001; Sungkorn et al. 2011). In the present work, the grid size was chosen according to the experimental energy spectrum.
In Figure 3, the energy spectrum of the vertical velocity was calculated from the measurement point in Figure 1 using a Fast Fourier Transformation (FFT). We have taken the energy spectrum from Akbar et al. (2012a) and transformed the x-axis from frequency to wavenumber with Taylor´s hypothesis of frozen turbulence. So the LES cut-off (filter size = 4mm) is shown in the transformed energy spectrum with dotted line. As can be seen the filter size is for Case 2 fine enough and for Case 1 it located

around at the beginning of the inertial subrange (Kolmogorov -5/3 range). Nevertheless, as in the section of results below shown, the vertical velocity fluctuation is in the order of the vertical mean flow, so the condition for using Taylor´s hypothesis $w'/\overline{w} \ll 1$ is actually not fulfilled. Nevertheless, the present approach provides some hint concerning the resolution.

Simulation Details

The inlet is defined as surfaces at the bottom of the domain, representing the experimental needle setup. The surface that represents one needle is rectangular with an edge length of 4x4 mm. The gas volume flow is divided equally over all needles. The inlet velocity is naturally equal to gas volume flow divided by the total inlet surface. At the walls, a no slip condition is applied for the continuous phase and a free slip condition for the dispersed phase. At the top of the column a degassing boundary is imposed, which means a slip condition for the continuous phase and an outlet for the dispersed phase. For the spatial discretization, a central difference scheme is employed, and a second order backward Euler scheme is used in time. The simulations were carried out using the time steps $\Delta t = 0.01 \cdots 0.015\ s$ to satisfy CFL < 1. The results were averaged over 250 s simulation time.

5. RESULTS

5.1 Instantaneous Results

In Figure 4, snapshots of streamlines taken from the inlet and the gas volume fraction at the centre plane are displayed for Case 2 as obtained with Eu-Eu-LES and Eu-Eu-URANS. So far, the bubbles reach the top of column, although the transient results changes. But the form and trend of the liquid velocity field and gas volume fraction are nearly similar in both, LES and URANS. The right graphs depict the concerning void fraction, showing a clear difference between the results for the two turbulence models. In the results shown with streamlines in Figure 4, the LES resolves much more of the details of the flow field. A large range of turbulence scales could be identified in the domain. With URANS, the transient details are not well resolved. It can be seen that only some large scale fluctuations are obtained, due to the high turbulent viscosity. Similar differences of the liquid velocity field with LES and URANS are also described by Deen et al. (2001) and Dhotre et al. (2008). This difference in liquid velocity field makes in the URANS simulation a more homogenous gas volume fraction distribution and the flow pattern not change so significant like LES.

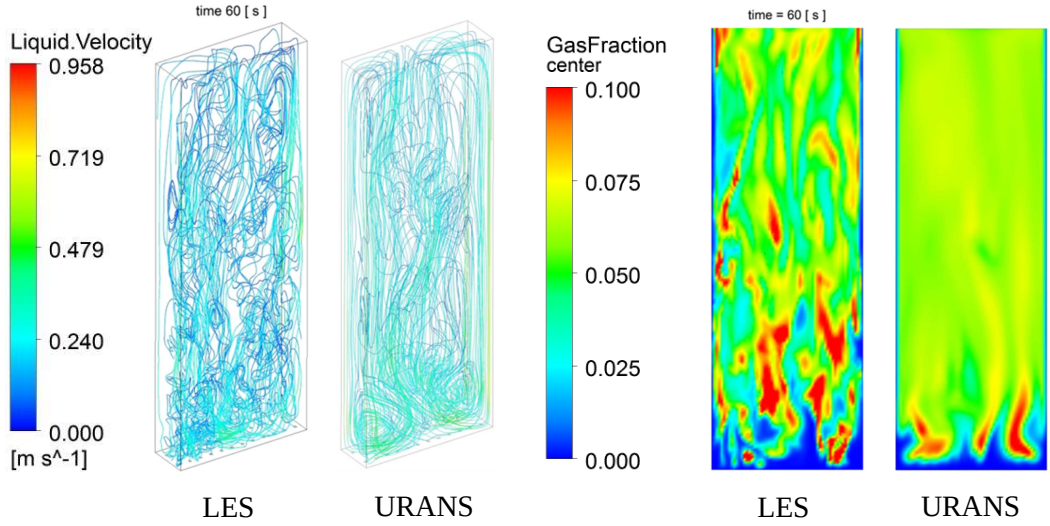

Fig. 4: Instantaneous data from Case 2 at 60 s. The left two graphs show instantaneous streamlines colored with the instantaneous absolute value of the liquid velocity. The right two graphs show the instantaneous void fraction in the centre plane.

5.2 Time-Averaged Results

In this section, the results from Eu-Eu-LES and Eu-Eu-URANS are compared with previous work (Akbar et al. 2012) using Euler-Lagrange LES (Eu-La-LES), which used a Lagrangian modelling for bubbles. The interfacial force models used in his work are comparable to the settings defined in Section 3.3, and the simulation was performed using two way coupling.

Long-time averaged vertical liquid velocity, gas volume fraction and vertical liquid velocity fluctuation are presented for both cases with experimental data of Akbar et al. (2012). All simulations presented were run for 250 s. All profiles were taken along the measurement line from wall to the centre at height of 500 mm, as represented by the broken line in Figure 1.

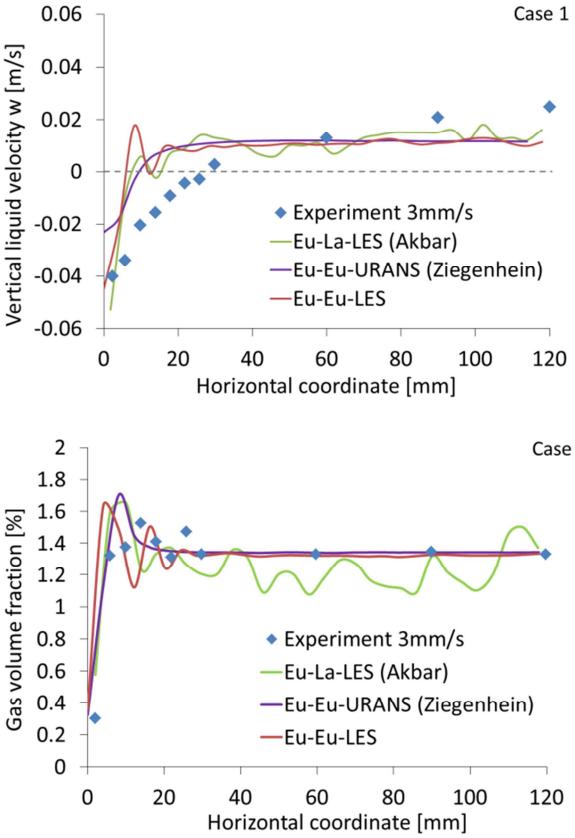

Fig. 5: Comparison of vertical liquid velocity (top) and gas volume fraction (bottom) for Case 1. Experimental data and Eu-La-LES are from Akbar et al. (2012). Eu-Eu-URANS are from Ziegenhein et al. (2014)

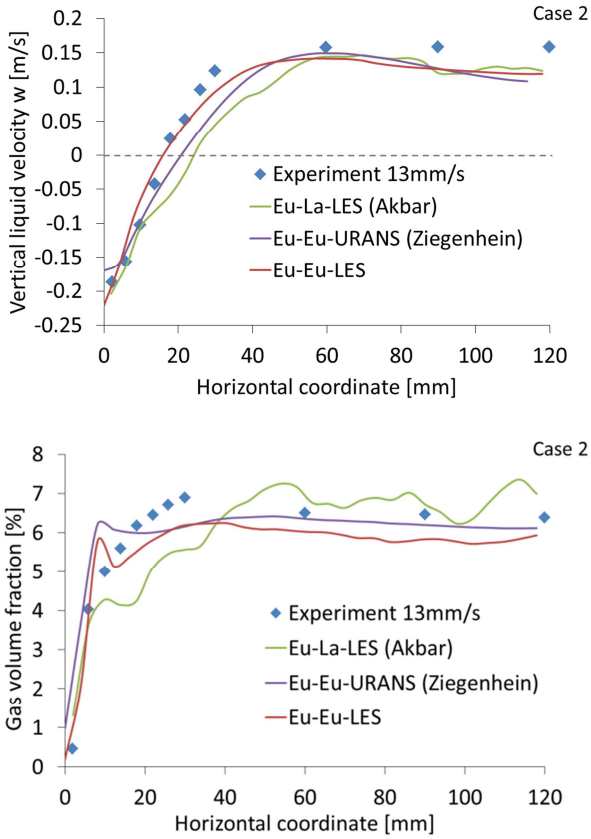

Fig. 6: Comparison of vertical liquid velocity (top) and gas volume fraction (bottom) for Case 2. Experimental data and Eu-La-LES are from Akbar et al. (2012). Eu-Eu-URANS are from Ziegenhein et al. (2014)

Figure 5 shows the vertical liquid velocity and gas volume fraction for Case 1. Quantitative agreement between all three simulations is obtained. The three predicted liquid velocity profiles are over predicted near the wall, but the nearly flat profiles in the core region are well reproduced. A peak near the wall in the experimental data in the void fraction profile in Figure 5 can be for all three simulations reproduced. This is also described by Krepper et al. (2007), who used a similar experimental facility. The gas volume fraction of about 1.2 % in the centre is obtained in all the simulations and the experimental data. The results from Akbar et al. (2012) using Eu-La-LES exhibits small oscillation at the averaged gas volume fraction and vertical liquid velocity in all results reported. The reason could be a somewhat too small averaging time.

In Figure 6, the results for high superficial gas velocity at the inlet (Case 2) are represented. A clear change in the direction of the liquid velocity can be seen at about 20 mm away from wall. This is a

phenomenon caused by liquid mass balance in the bubble column, obtained in all three predictions with a quite good quantitative agreement. In the near wall region of velocity profile, the results with Eu-Eu-LES match the experimental data better than the other two simulations. For the gas volume fraction profile in Figure 6, all the predicted values give good agreement with the experimental data. A small peak near the wall can be obtained again in the Eu-Eu-LES. This peak caused by the lift force modelling making the small bubbles go towards to the wall, and migrate the big bubbles to the centre, this caused the slight second peak in the position about 40 mm away from the wall. The same phenomenon appears also in the URANS simulation with using the same lift force modelling. The gas volume fraction results of Eu-La-LES underpredict the void fraction near the wall region and generally exhibit a very jaggy profile, presumably due to lack of averaging.

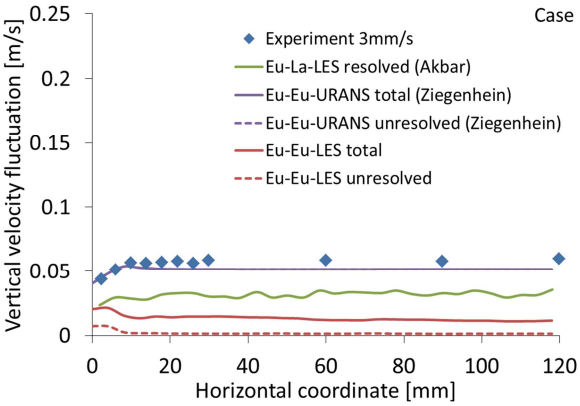

Fig. 7: Comparison of vertical liquid velocity fluctuation for Case 1. Experimental data and Eu-La-LES are from Akbar et al. (2012). Eu-Eu-URANS are from Ziegenhein et al. (2014)

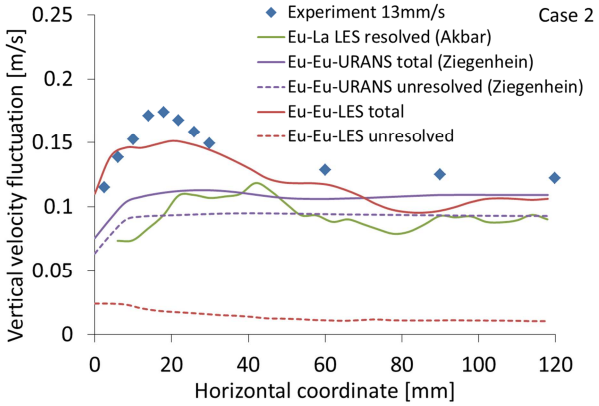

Fig. 8: Comparison of vertical liquid velocity fluctuation for Case 2. Experimental data and Eu-La-LES are from Akbar et al. (2012). Eu-Eu-URANS are from Ziegenhein et al. (2014)

Figure 7 and Figure 8 show comparisons between experimental and predicted vertical liquid velocity fluctuation for Case 1 and Case 2, respectively. With the Eu-La-LES only the resolved velocity fluctuation is provided in Akbar et al. (2012), the unresolved part is neglected. At this point, in our Eu-Eu-LES the total vertical velocity fluctuation is considered, which could be decomposed in resolved part $\overline{w}''$ and unresolved part w' as be mentioned in Section 3.2. For the resolved part, $\overline{w}''\overline{w}'' = [\overline{w} - \langle\overline{w}\rangle]^2$ is computed using the difference between the resolved vertical velocity and the time average of the resolved vertical velocity. For the unresolved part, as can be seen in (4), only the anisotropic part of the SGS stress tensor is considered in the Smargorinsky model, so that the information about isotropic part $\tau_{kk} = 2k$ is lost. Dhotre et al. (2013) performed a review about application of LES to dispersed bubbly flows, observing that in all papers collected SGS kinetic energy k_{sgs} was neglected when zero equation models were used in LES. Only Niceno et al. (2008) demonstrated the applicability of one-equation model for k_{sgs}, so that k_{sgs} could be explicitly calculated. Here, a method for estimating k_{sgs} will be introduced as following, with ε_{sgs} is dissipation in SGS:

Using k-ε Model approach

$$K_{sgs} = \sqrt{\frac{\nu_{sgs}\varepsilon_{sgs}}{C_\mu}}, \quad \varepsilon_{sgs} = \nu_{sgs}\,|\bar{S}|^2. \tag{7}$$

This method for estimation the SGS kinetic energy based on calculation of the local turbulent dissipation in SGS. The evaluation of the subgrid contributions improves the prediction of the total velocity fluctuation.

As can be seen in Figure 7, for Case 1 both LES with Euler-Euler and Euler-Lagrangian have much lower values than the experimental data. The unresolved part from Eu-Eu-LES is quite small and has nearly no influence on the evaluation. The cause of the underprediction can be related to the filter feature of LES and can be explained, that the largest fluctuation in w is caused in the vicinity of bubbles (Risso et al. 2001), only the liquid velocity averaged over the computational cell ($d^*\sim1$ in this case) is however dealt with in LES. With the Eu-Eu-URANS the experimental data can be very good reproduced. Nevertheless the total and unresolved vertical fluctuation profiles are nearly the same. Therefore, the resolved fluctuations using the Eu-Eu-URANS method are zero for Case 1. Hence, all the velocity fluctuations come from the used two equation turbulence model with the BIT model. Summarizing, this might be a hint that the large fluctuations are in general very low in Case 1 and the bubble induced turbulence is dominant. Because the used bubbly flow subgrid models for the Eu-Eu-LES method include only dissipation terms, as mentioned in Section 3.2, the total velocity fluctuations with this method might be underpredicted

Figure 8 shows velocity fluctuation for Case 2. In this case, higher large scale turbulence is expected, because of the higher superficial velocity. The result of the Eu-Eu-LES has a quantitative better agreement with the measured data than the other two simulations shown in Figure 8. Especially the measured peak is only reproduced by the Eu-Eu-LES and located at the change of sign of the vertical liquid velocity, as mentioned in Figure 6. The unresolved velocity fluctuation obtained by using the Eu-Eu-LES method in Figure 8 contains about 10% of the total velocity fluctuations. The result with Eu-La-LES underpredicts the fluctuation in this case, which might be caused by neglecting the unresolved part. The trend of a peak close to the wall can also be found in the resolved part of Eu-La-LES.

The results from Eu-Eu-URANS fit the measured profile although well in both cases in Figure 7 and 8. However the application of URANS with a two equation turbulence model for prediction of velocity fluctuation in one direction might be critic. Because the isotropic assumption of turbulence leads to $\overline{w'w'} = \overline{v'v'} = \overline{u'u'} = \frac{2}{3}k$. For Case 1, the profile of total velocity fluctuation and the unresolved part are nearly totally overlapped, which means, as discussed above, nearly no turbulence is resolved in Case 1. Similarly in Figure 8 for Case 2, the unresolved part contributes almost 90% of the total fluctuation. So the lateral velocity fluctuations in the other two directions in both cases would have nearly the same profiles like the vertical direction. Therefore, it might be a problem at this point that only one velocity component is evaluated for the Eu-Eu-URANS approach. The previous work from Dhotre et al. (2008) mentioned also the limit of URANS models to predict the liquid velocity fluctuation in one direction. The comparison between the total turbulent kinetic energy and experimental data could give a better agreement. Unfortunately, the experimental data consists only of one velocity fluctuation component.

5.3 The Energy Spectrum

In Figure 9 for Case 2, a 200 s time history plot of the resolved vertical liquid velocity at the centre of the measurement line (Figure 1) from Eu-Eu-LES is shown, with 20000 sample points.

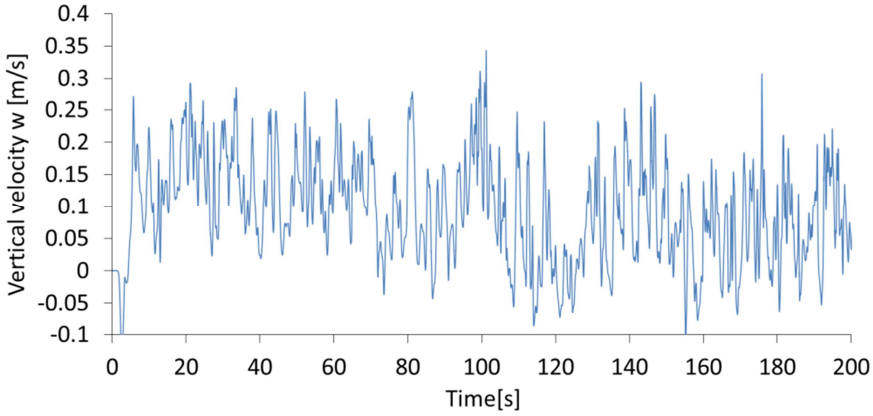

Fig. 9: Time history of the liquid velocity obtained with Eu-Eu-LES at the centre of measurement line for Case 2

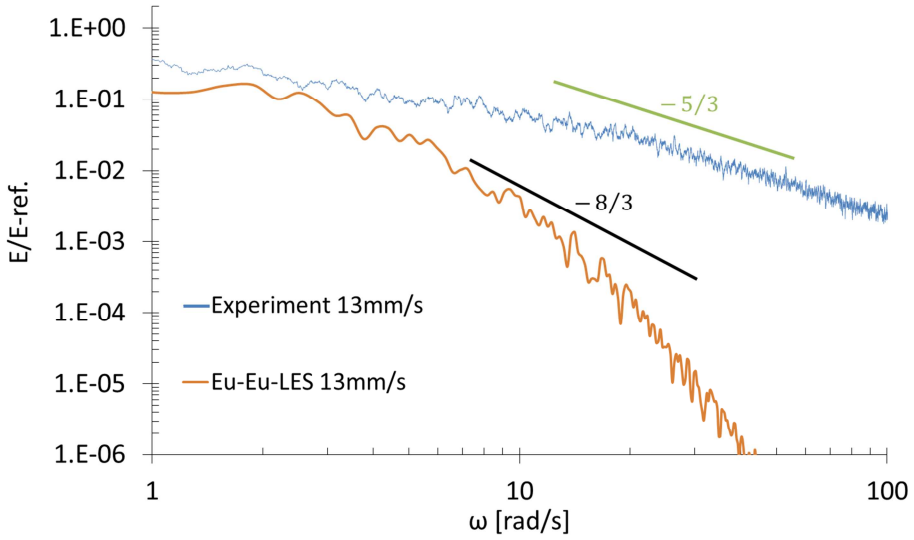

Fig. 10: Energy spectrum of vertical liquid velocity scaled with an arbitrary reference value

The energy spectrum obtained with the data extracted from Figure 9 is shown in Figure 10. The velocity signal using the Welch method (Welch 1967) with 10 non overlapping windows was performed. Each window contains 2000 sample points, and a Hanning window function was used. As can be seen, the turbulent energy spectrum with the Eu-Eu-LES approach exhibits a broad range of frequency, with a slope changing even steeper than the still in discussion two-phase -8/3 power laws in the inertial subrange (Mercado et al. 2010). A similar energy spectrum based on the Eu-Eu-LES results is also obtained by Dhotre et al. (2008). In his work the slope was partly even over -10/3 in the inertial subrange.

Previous experimental studies have actually attributed the more dissipative spectrum to the presence of the bubbles, this being responsible for eddy disintegration (Lance et al. 1991). But in the experimental energy spectrum for Case 2 of Akbar et al. (2012), an expected more dissipative slope does not appear in Figure 10. The difference between the Eu-Eu-LES energy spectrum and the experimental energy spectrum could be caused by many different reasons. A determinant reason might be the limitations caused by the Euler-Euler approach. It might not be able to reproduce a similar power law like experimental one. Since in the Euler-Euler approach, there is no bubble resolved, it is impossible to catch the frequency information in the bubble wake like in the experiment.

6. CONCLUSIONS

The Eu-Eu-LES have been carried out for the rectangular bubble column and compared with the experimental data from Akbar et al. (2012), the previous work with Eu-La-LES (Akbar et al. 2012) and Eu-Eu-URANS (Ziegenhein et al. 2014). The BIT was taken into account in Eu-Eu-LES using the Sato model.

In general, with the Eu-Eu-LES very good results can be achieved. The results obtained with the Eu-Eu-LES approach reproduce the measured gas volume fraction and liquid velocity profiles in the same way as Eu-La-LES (Akbar et al. 2012) and Eu-Eu-URANS (Ziegenhein et al. 2014). Large improvement can be achieved with the Eu-Eu-LES method for the turbulence prediction in the case with a higher gas superficial velocity. A near wall peak in the velocity fluctuation can be reproduced. For lower gas superficial velocity, LES may not represent the best option for turbulence prediction in this case, since large-scale turbulence is not present for the case of lower gas superficial velocity.

The criterion for a suitable cut-off is discussed. It could be obtained from the experimental energy spectrum in the wavenumber space, the chosen cut-off for the high superficial velocity is fine enough. However, for the one with a low gas superficial velocity the cut-off might be too coarse. That might cause the underprediction of the velocity fluctuation for the case with a low gas superficial velocity in both Eu-Eu-LES and Eu-La-LES.

A method for estimating SGS kinetic energy is introduced and investigated. It could be obtained, considering this unresolved part can improve the prediction of the velocity fluctuation. A similar

power law like experimental energy spectrum might not be able to be reproduced with Eu-Eu-LES, since the bubbles are not resolved in Euler-Euler approach and the frequency information in bubble wake is lost. Further tests of such combination of interfacial force models and the treatment of turbulence proposed here applying it to different bubbly flows are desired and will be conducted in the future.

ACKNOWLEDGEMENTS

This work is carried out in the frame of a current research project funded by the German Federal Ministry of Economic Affairs and Energy, project number 150 1411.

REFERENCES

M.H.M. Akbar, K. Hayashi, S. Hosokawa, A. Tomiyama "Bubble Tracking Simulation of Bubble-induced Pseudo Turbulence", *6th Japanese-European Two-Phase Flow Group Meeting*. 2012a.

M.H.M. Akbar, K. Hayashi, S. Hosokawa, A. Tomiyama "Bubble tracking simulation of bubble-induced pseudo turbulence", *Multiphase Science and Technology* 24, 197- 222 (2012).

N. G. Deen, B. H. Hjertager, and T. Solberg "Comparison of PIV and LDA measurement methods applied to the gasliquid flow in a bubble column", in *Proceedings of the 10th International Symposium on Applications of Laser Techniques to Fluid Mechanics*, Lisbon, Portugal, July 2000.

N. G. Deen, T. Solberg, and B. H. Hjertager "Large eddy simulation of the gas-liquid flow in a square cross-sectioned bubble column", *Chemical Engineering Science*, vol. 56, no. 21-22, pp. 6341–6349, 2001.

M.T. Dhotre, B. Niceno, and B. L. Smith "Large eddy simulation of a bubble column using dynamic sub-grid scale model," *Chemical Engineering Journal*, vol. 136, no. 2-3, pp. 337–348, 2008.

M.T. Dhotre, N. G. Deen, B. Niceno, Z. Khan, and J. B. Joshi "Large Eddy Simulation for Dispersed Bubbly Flows: A Review", *International Journal of Chemical Engineering*, vol 2013, 2013.

S. Hänsch, D. Lucas, E. Krepper and T. Höhne "A multi-field two-fluid concept for transitions between different scales of interfacial structures", *Int. J. Multiphase Flow*, vol. 47, pp. 171–182, 2012.

S. Hosokawa, A. Tomiyama, S. Misaki, and T. Hamada, "Lateral Migration of Single Bubbles Due to the Presence of Wall", *Proc. ASME Joint U.S.-European Fluids Engineering Division Conference*, FEDSM2002, Montreal, Canada, 855, 2002.

M. Ishii, N. Zuber, "Drag Coefficient and Relative Velocity in Bubbly, Droplet or Particulate Flows", AlChE Journal, vol. 25, 843 (1979).

J.B. Joshi, N.S. Deshpande, M. Dinakar, D.V. Phanikumar "Hydrodynamic stability of multiphase reactors", *Advances in Chemical Engineering*. Academic. vol. 26, p. 1, 2001.

E. Krepper, B.N.R. Vanga, A. Zaruba, H.-M. Prasser and M.A. Lopez de Bertodano "Experimental and numerical studies of void fraction distribution in rectangular bubble columns", *Nuclear Engineering and Design*, vol. 237, 399 (2007).

E. Krepper, D. Lucas, T. Frank, H. M. Prasser, P. Zwart "The inhomogeneous MUSIG model for the simulation of polydispersed flows", *Nuclear Engineering and Design*, vol. 238, 1690-1702 (2008).

M. Lance, J. Bataille "Turbulence in the liquid phase of a uniform bubbly air-water flow", *J. Fluid Mech.* 222, 95–118 (1991).

J.M. Mercado, D. C. Gomez, D. Van Gils, C. Sun and D. Lohse "On bubble clustering and energy spectra in pseudo-turbulence", *J. Fluid Mech*, vol. 650, pp. 287-306, 2010.

M. Milelli, B. L. Smith, and D. Lakehal "Large-eddy simulation of turbulent shear flows laden with bubbles", in *Direct and Large-Eddy Simulation-IV*, B. J. Geurts, R. Friedrich, and O. Metais, Eds., vol. 8 of *ERCOFTAC Series*, pp. 461–470, Kluwer Academic Publishers, Dordrecht, The Netherlands, 2001.

B. Niceno, M.T. Dhotre, and N.G. Deen "One-equation subgrid scale (SGS) modelling for Euler-Euler large eddy simulation (EELES) of dispersed bubbly flow", *Chemical Engineering Science*, vol. 63, no. 15, pp. 3923–3931, 2008.

F. Risso, K. Ellingsen “On the Rise of an Ellipsoidal Bubble in Water: Oscillatory Paths and Liquid-induced Velocity”, *Journal of Fluid Mechanics*, vol. 440, pp. 235–268, 2001.

R. Rzehak, E. Krepper “Bubble-induced turbulence: Comparison of CFD models”, *Nuclear Engineering and Design* 258, 57-65, 2013.

Y. Sato, M. Sadatomi, and K. Sekoguchi “Momentum and heat transfer in two-phase bubble flow-I. Theory”, *International Journal of Multiphase Flow*, vol. 7, no. 2, pp. 167–177, 1981.

M.L. Shur, P.R. Spalart, M.K. Strelets, and A.K. Travin, “A hybrid RANS-LES approach with delayed-DES and wall-modeled LES capabilities”, International Journal of Heat and Fluid Flow 29, pp. 1638-1649 (2008).

J. Smagorinsky “General circulation experiments with the primitive equations”, *Monthly Weather Review*, Vol. **91**, no. 3, pp. 99–165, 1963.

R. Sungkorn, J. J. Derksen, and J. G. Khinast “Modeling of turbulent gas-liquid bubbly flows using stochastic Lagrangian model and lattice-Boltzmann scheme”, *Chemical Engineering Science*, vol. 66, no. 12, pp. 2745–2757, 2011.

A. Tomiyama, H. Tamai, I. Zun, S. Hosokawa, “Transverse migration of single bubbles in simple shear flows”, Chemical Engineering Science, vol. 57, 1849 (2002).

P.D. Welch, "The Use of Fast Fourier Transform for the Estimation of Power Spectra: A Method Based on Time Averaging Over Short, Modified Periodograms", *IEEE Transactions on Audio Electroacoustics*, AU-15, 70–73, 1967.

T. Ziegenhein, R. Rzehak and D. Lucas, “Transient simulation for large scale flow in bubble columns”, submitted to *Chemical Engineering Science*, 2014.